Journal of Applied Physics ARTICLE scitation.org/journal/jap

Effects of acoustic softening on thermal conductivity beyond group velocity

Cite as: J. Appl. Phys. **127**, 204302 (2020); doi: 10.1063/1.5135584
Submitted: 6 November 2019 · Accepted: 6 May 2020 ·
Published Online: 27 May 2020

View Online Export Citation CrossMark

M. D. Gerboth[1] and D. G. Walker[2,a)]

AFFILIATIONS

[1]Interdisciplinary Materials Science, Vanderbilt University, Nashville, Tennessee 37215, USA
[2]Department of Mechanical Engineering, Vanderbilt University, Nashville, Tennessee 37215, USA

[a)]**Author to whom correspondence should be addressed:** greg.walker@vanderbilt.edu

ABSTRACT

We model the highly reduced thermal conductivity of nanostructured materials observed in nanoribbons. For highly scaled structures, such as wires with diameters on the order of 20 nm, physical effects beyond classical boundary scattering, including acoustic softening, become important. To date, work on acoustic softening has focused on reductions in group velocity. However, a reduction in the group velocity implies that the phonon dispersion is modified. Here, we investigate how changes in the phonon dispersion manifest in the mean free path, heat capacity, and group velocity. Including these effects in the modeling of thermal conductivity, we find that softening increases low-temperature thermal conductivity while reducing high temperature thermal conductivity. We further compare the model to experimental data.

I. INTRODUCTION

Physical effects beyond classical boundary scattering become important to thermal transport in highly scaled nanostructured materials. Previous work by Yang *et al.*[1] provided measurements of the thermal conductivity for individual silicon nanoribbons of various sizes and aspect ratios. Their results and analysis suggest that multiple size-dependent effects contribute to the reduced thermal conductivity of nanoribbons at scales below where classical boundary effects dominate. In particular, acoustic softening, which occurs because of the influence of the atomic coordination near the surface, alters the thermal transport properties and becomes significant in extremely scaled devices.

Initial measurements of single nanowires by Li *et al.* demonstrated that the thermal conductivity was significantly reduced from the bulk value.[2] For wires with diameters greater than 22 nm, the reduced thermal conductivity could be explained through classical surface scattering effects. However, for 22 nm wires, classical explanations did not suffice and deviations from a T^3 low-temperature dependence were found. Further work by Chen *et al.* measured the thermal conductance of similarly thin CVD grown silicon nanowires with diameters ranging from 15 nm to 50 nm.[3] The measurements confirmed the deviation from a T^3 low-temperature dependence, which Chen *et al.* attributed to frequency-dependent boundary scattering; however, their model consistently predicted higher thermal conductivity near room temperature than observed. Work by Wingert *et al.* using Ge and Ge–Si core-shell nanowires with diameters of 20 nm additionally observed highly reduced thermal conductivity and modifications to the temperature dependence of thermal conductivity.[4] They found an enhancement to thermal conductivity at low temperature and a reduction about room temperature for the Ge–Si core-shell nanowires.

Subsequent work by Wingert *et al.* examining crystalline Si nanotubes found thermal conductivities below the limit for boundary scattering and below measured values for amorphous silicon.[5] To explain these highly reduced thermal conductivities, Winger *et al.* proposed acoustic softening. Building on theoretical and experimental evidence of the size dependence of the elastic modulus in nanostructures, Wingert *et al.* hypothesized that the phonon group velocity, which is proportional to the elastic modulus, may be reduced for small wires leading to significant contribution to reduced thermal conductivity. They additionally measured significantly reduced elastic moduli for their Si nanotubes using nanoscale tensile tests, lending credence to the acoustic softening hypothesis.

Thermal conductivity can be approximated as $\kappa = \frac{1}{3} C_v v l$, where v is the phonon group velocity and l is the mean free path (MFP). In nanostructures, reduced thermal conductivity is usually attributed to a reduced MFP arising from surface scattering; in

contrast, acoustic softening causes additional reductions in the thermal conductivity of nanostructures that arise from a reduction in v. In the continuum limit, the speed of sound (and thus the long wavelength phonon group velocity) is proportional to $\sqrt{E}$, where E is Young's modulus, implying that a softening of the material should induce a reduction in the phonon group velocity.

One of the early theoretical explanations for the size dependence of Young's modulus is the effect of surface strain energy contribution to the energy of the structure.[6] When deformed elastically, structures store energy in both the bulk and the surface but at different rates. When the surface area-to-volume ratio becomes sufficiently large, surface elasticity contributes significantly to the effective elastic modulus. Studies of the elastic modulus of nanostructures employing molecular dynamics and *ab initio* methods have found good qualitative agreement with this theory,[7–12] but numerical analyses tend to predict the onset of softening to occur at much smaller sizes than observed in experiments. To reconcile the discrepancies between theoretical calculations and experimental work, a number of explanations have been proposed, including native oxide layers[13–15] and manufacturing defects.[14,16]

Additionally, experimental observations of size-dependent reductions in the effective elastic modulus have been reported for a number of silicon nanostructures, including wires[13,17–19] and cantilevers.[14,20] Yang *et al.* measure the effective elastic modulus for nanoribbons similar to the ones that were measured for thermal conductivity,[1] further confirming the link between reduced thermal conductivity and acoustic softening. Despite this work, the mechanisms and consequences of acoustic softening on thermal conductivity (especially the temperature dependence of the thermal conductivity) have yet to be fully elucidated.[21]

In this paper, we explore how acoustic softening may be incorporated into simple thermal conductivity models to give good estimates of the size-dependent thermal conductivity for nanoribbons. More importantly, we have identified a number of competing effects that arise when including softening in the models. In particular, changes to the effective stiffness of a material should have effects not only on the speed of sound, which is approximated as the phonon group velocity at the gamma point but also the group velocity across the dispersion relation. Additionally, through the altered dispersion relation, scattering rates and heat capacity may also be altered. Thus, we argue that the size dependence of thermal conductivity in structures experiencing size-dependent softening likely arises from a combination of these mechanisms, which may also give rise to changes in the temperature dependence of the thermal conductivity.

II. THERMAL CONDUCTIVITY MODEL

To model the thermal conductivity of nanoscale ribbons, consider the frequency-dependent Landauer-like equations proffered by Callaway and Holland,

$$\kappa = \frac{1}{3}\int C_v(q) v_g(q) F_g(q) l(q) dq, \tag{1}$$

where the mean free path and specific heat are approximated as such:

$$l(\omega) = v_g(\omega)\left[\frac{v_g(\omega)}{b} + A\omega^4 + P\omega^2 T \exp\left(\frac{-C_u}{T}\right)\right]^{-1}, \tag{2}$$

$$C_v(q) = \frac{3\hbar^2}{2k_B\pi^2}\frac{1}{T^2}\frac{q^2\omega^2(q)e^{\hbar\omega(q)/k_BT}}{\left(e^{\hbar\omega(q)/k_BT}-1\right)^2}. \tag{3}$$

Here, v_g is the group velocity, and F_g is a reduction factor for the MFP based on surface scattering. All of the terms in Eq. (1) are dependent on the dispersion through the wavevector q. The bulk-like phonon MFP ($l(\omega)$) includes terms for grain boundary scattering ($v_g(\omega)/b$), impurity scattering ($A\omega^4$), and phonon–phonon scattering ($P\omega^2 T \exp(-C_u/T)$). Scattering rates of this form have been widely used to model thermal conductivity; however, these rates rely on fitting parameters. Further, these forms are derived from a long wavelength approximation ignoring the effect of optical modes. More recent work calculating relaxation times using *ab initio* methods[22] have succeeded in modeling the thermal conductivity of silicon. These studies have indicated that at high frequencies, the dependence on the scattering rate deviates from the ω^2 dependence used here, driven by the ω^4 dependence of Umklapp scattering, and the scattering matrix differs significantly from the long wavelength approximation for frequencies above a critical frequency.[22] Despite this, we continue to use the above terms for scattering rate as the exact form should have a limited effect on the overall results. Previous studies of size effects have focused on F_g, which encapsulates the effect of surface scattering. Additional size effects enter through v_g, where size-dependent softening reduces the group velocity. For the heat capacity (C_v) and the MFP (l), the size dependence is more indirect, arising from the modification to phonon frequencies (and energies) that is implied by softening of the dispersion.

For a softened dispersion relation, we use the BvKS (Born-von Karman-Slack) model, a quarter sine wave, with parameters that were found to reproduce the bulk thermal conductivity of silicon.[23,24] Softening is incorporated into the model by modifying the dispersion relation so that it becomes

$$\omega = \frac{2}{\pi}F_s v_b q_0 \sin\left(\frac{\pi q}{2q_0}\right), \tag{4}$$

where F_s is proportional to the ratio of the softened speed of sound to the bulk speed of sound v_b. For the maximum reductions in Young's modulus reported in the literature,[1,5,17,19,20,25] this ratio ranges as low as $F_s = 0.4$ to $F_s = 0.8$ for the smallest measured structures, but assumes values up to $F_s = 1$ for an unsoftened (bulk) wire. A review of size-dependent mechanical properties indicates that there is a high degree of scatter in the size-dependent Young's moduli reported from experiment,[26] and the theoretical work predicted that softening should not be significant until smaller sizes than seen in experiment.[14,16] For this work, we determine F_s by fitting the data from Yang *et al.*[1] for Young's modulus vs hydraulic diameter. Yang *et al.* have reported both Young's modulus and thermal conductivity for sets of Silicon nanoribbons.

We fit Young's modulus with the function

$$E = \frac{E_{\text{bulk}}}{1 + \exp[-k(d_h - d_0)]}, \tag{5}$$

where k and d_0 are fitting parameters related to the slope of the decreasing Young's modulus and the diameter, where $E/E_{\text{bulk}} = 0.5$, respectively. E_{bulk} is the bulk Young's modulus. The fit (Fig. 1) results in $k = 0.240\,\text{nm}^{-1}$ and $d_0 = 25.9\,\text{nm}$. E_{bulk} for the fit is 176.8 GPa, which is in line with experimental and theoretical values for silicon.[15,27,28] The sound speed reduction factor is then defined as

$$F_s = \sqrt{\frac{E_{\text{nano}}}{E_{\text{bulk}}}} = \sqrt{\frac{1}{1 + \exp\left[-k(d_h - d_0)\right]}}. \tag{6}$$

We note that in this definition the fitted bulk modulus cancels out. From this, we find that $F_s = 0.55$ corresponds to a hydraulic diameter of approximately 22 nm.

Using these softened phonon frequencies, the effects of softening can be incorporated into the MFP and heat capacities, as well as the group velocities. The consequences of these physical effects are explored below.

A. Group velocity

Changes in group velocity are the most obvious factor that occurs with acoustic softening. From a continuum point of view, the presence of a dominating surface alters the elastic-modulus resulting in an effective modulus (E_{nano}) for the nanostructure. The speed of sound in the nanostructure is then related to the effective modulus as $v_s = \sqrt{\frac{E_{\text{nano}}}{\rho}}$. Therefore, if the effective modulus is reduced in a nanostructure because of the surface softening, so too should the group velocity. However, this reduction implies that there should be a reduction in the group velocity not only at the gamma point but also across the entire first Brillouin zone (FBZ). More explicitly, a reduction in the elastic modulus reduces both the slope of the dispersion (group velocity) at the center of the FBZ and the phonon frequencies at the edge of the FBZ, which are also proportional to $\sqrt{E_{\text{nano}}}$.

B. Mean free path

A less obvious factor that may be affected by acoustic softening is the mean free path. In nano-structured devices, the MFP is controlled by multiple features: surface scattering, grain boundary scattering, impurity scattering, and phonon–phonon scattering. For both surface scattering and grain-boundary scattering, the MFP is set by the geometry of the scattering surfaces, i.e., the geometry of the object, included through F_g, which is calculated from Monte Carlo ray tracing (MCRT) discussed in Sec. I, and grain size, respectively. As the nanostructures we are interested in are formed via epitaxy, grain-boundary scattering should result in a relatively small influence on the overall MFP and will be ignored. Additionally, grain-boundary scattering is not sensitive to softening effects.

1. Geometric boundary scattering

For structures with a single dominant dimension, e.g., films and wires, the characteristic length is used directly to estimate the boundary scattering. In structures that have more than one governing dimension, we have several options. First, we can use an effective size, such as a Casimir length. Second, all device dimensions can be included through Mathieson's rule. And finally, we can use

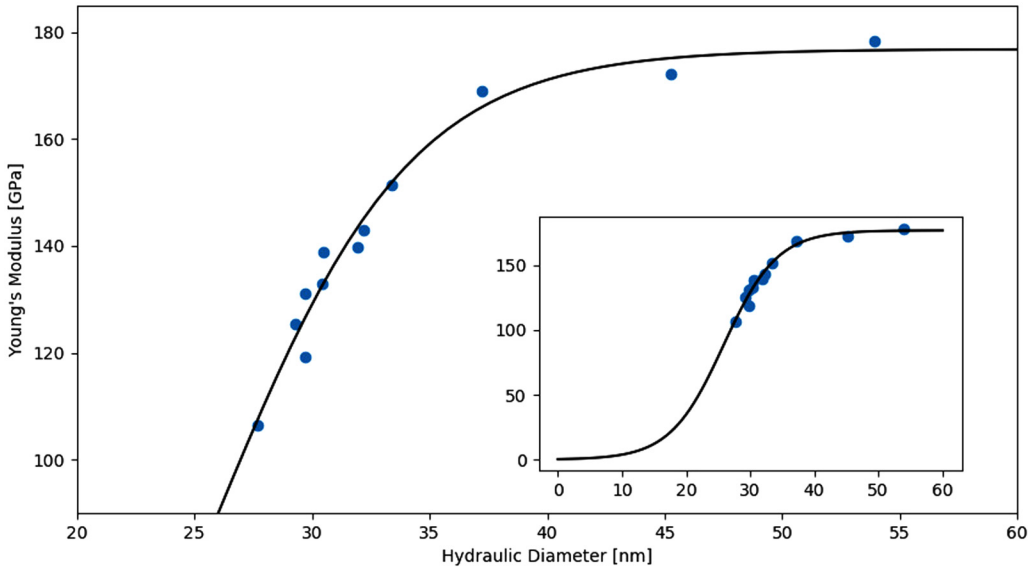

FIG. 1. Fit of Young's modulus vs hydraulic diameter for nanoribbons from Yang *et al.*[1] Inset: fit extended to 0 nm hydraulic diameter.

a more detailed model of the scattering, such as Monte Carlo ray tracing, that rigorously accounts for several effects, such as corners and specularity. To compare results from our softened thermal conductivity model with nanoribbons, such as those produced by Yang *et al.*, we use the final method as the presence of two dominant dimensions (width and height) reduce the accuracy of the first two options. Parametric sweeps of thick ribbons with aspect ratios from 1 to 15 (similar to the aspect ratios seen in Ref. 1) have been reported by Park *et al.*[29] and indicate that for structures between these ratios, the aspect ratio must be included in modeling the geometric reduction of thermal conductivity. In this regime, both cross sectional dimensions strongly influence the resulting MFP, and considerations such as corner effects become important, so we use MCRT to model boundary scattering. While it provides accurate boundary scattering, the MCRT method can be computationally intensive; so, to isolate and rapidly explore the effects of modifying the dispersion relation on thermal conductivity, we also present systems that include a single characteristic dimension.

In the MCRT approach, a calculated geometric factor $F_g(q, w, h) = \Lambda_n(q)/\Lambda_b(q)$ is the ratio of the actual nanostructure mean free path dictated by the boundaries scaled by the mean free path in a bulk material. The MCRT procedure takes its inspiration from the well known Fuchs–Sondheimer (FS) formalism[30,31] first used to describe electrical conductivity in thin films and later widely used to treat phonons.[1,29,32] Under the Fuchs–Sondheimer (FS) formalism, the geometric reduction arises from the influence of a (partially) diffuse surface on the MFP of a carrier (e.g., an electron). At any point in the structure, the influence of a surface at some distance from that point will cause a reduction in the mean free path due to the change in particle momentum when scattered off the surface. By integrating over all interior points and all directions to the surface, the reduction in the mean free path can be computed.

In our case, we have replaced the integration in the FS model with a MCRT procedure following McGaughey.[33] This replacement allows us to incorporate specularity and other geometric features into our model not directly available in the FS model. The procedure, outlined in Fig. 2, is as follows. First, a free flight distance d_{free} is pseudo-randomly selected from an exponential distribution with a mean of l_{bulk} and an initial direction is pseudo-randomly selected. In the second step, ray tracing is employed to determine the distance (l) from the initial point to the surface along the selected direction. If $d_{\text{free}} < l$, then the free path for that trial is d_{free}. If $d_{\text{free}} > l$, then we treat the interaction with the surface as either diffuse or specular. The selection is made pseudo-randomly based on the specularity parameter p: the fraction of specular events. The parameter p ranges from 0 (entirely diffuse) to 1 (completely specular) and is treated as a free parameter in the simulation. In the diffuse case, the free path for the trial is l. For specular events, a new direction is chosen by inverting the directional component normal to the surface, and ray tracing is continued with $d_{\text{free}} = d_{\text{free}} - l$ until either a diffuse event or d_{free} is reduced to below zero. In the case of ray tracing with specular reflections, the free path for the trial is the sum of all the ray lengths $l = l_1 + l_2 + \cdots + l_n$. Additional trials are calculated using the final position of the previous trial as the starting position for the new trial, and the reduced MFP is calculated as the average of the free

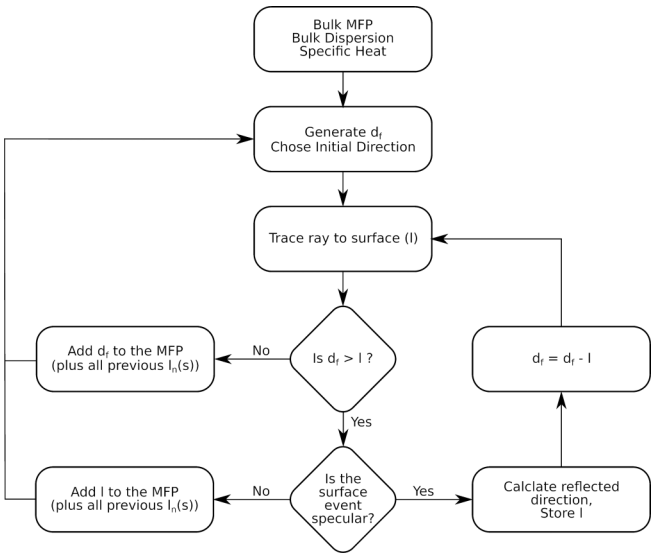

FIG. 2. MCRT procedure.

paths of all the trials. For a specularity of 1 (i.e., no surface scattering), the MCRT calculations recover an $F_g = 1$, verifying the model. For the calculations in this report, we consider the limiting case of a fully diffuse boundary ($p = 0$).

2. Impurity and phonon–phonon scattering

While grain boundary and geometric surface scattering are not affected by acoustic softening, impurity and phonon–phonon scattering can be. As both of these scattering rates have a nonlinear dependence on the frequency (usually modeled as a power law), the effects on the scattering rate of a modification to the dispersion relation persist in the contribution to the MFP term resulting from both these phenomena.

To demonstrate this more clearly, we consider the Callaway models for scattering. These power law formulas, which we use for scattering, are[23,24,34]

$$\tau_I^{-1}(\omega) = A\omega^4, \tag{7}$$

$$\tau_{pp}^{-1}(\omega) = P\omega^2 T \exp\left(\frac{-C_u}{T}\right), \tag{8}$$

where A, P, and C_u are fitting parameters that depend on the material and phonon branch and are taken from the literature,[23,24] where they are found to reproduce bulk Si thermal conductivity well. At the nanoscale, the choice of parameters should not have a large effect on our results as surface scattering will dominate. We do not include terms for normal scattering, and thus results for scattering at low temperatures should be viewed with caution. However, at low temperatures, the thermal conductivity is dominated by the heat capacity. Formulating these relations as MFPs

then introduces the dispersion relation through the group velocity,

$$l_I(\omega) = \frac{v_g(\omega)}{A\omega^4}, \tag{9}$$

$$l_{pp}(\omega) = \frac{v_g(\omega)}{P\omega^2 T \exp\left(\frac{-C_u}{T}\right)}. \tag{10}$$

Therefore, a modified dispersion due to acoustic softening will alter the MFP. This effect is captured in the MCRT.

For phonon–phonon softening, in addition to the group velocity ($v_g(\omega)$) and the frequency (ω), the fitting parameters are also modified by softening. The factor P can be expressed as $P = \frac{\hbar\gamma^2}{Mv^2\Theta_D}$.[35] The Debye temperature, Θ_D, and the Grüneisen parameter, γ, are both proportional to the softening fraction F_s. This leads to a dependence on the softening factor of $1/F_s$ for P. Additionally $C_u \propto \Theta_D$. Thus, for the phonon–phonon scattering, the softened phonon–phonon scattering is

$$\tau_{pp}^{-1}(\omega) = F_s P \omega_b^2 T \exp\left(\frac{-F_s C_u}{T}\right), \tag{11}$$

where ω_b is the unsoftened phonon frequency.

For impurity scattering, a softened dispersion results in an increase in the MFP across the FBZ. This is in contrast to the phonon–phonon scattering. In this case, the P parameter, the frequency, and the group velocity softening dependencies cancel out, leaving only the effect of softening on C_u. This results in a small decrease in the MFP from softening. For the $\tau \propto \frac{1}{\omega^4}$ behavior calculated by Ward and Broido,[22] the frequency dependence on softening would in contrast cause an increase in the MFP. As discussed below in and seen in Fig. 4, the difference between the two models, when incorporating surface scattering, should be small.

To examine the combined effects of impurity and phonon–phonon scattering, we use a system without surface scattering (where the only geometric scattering included is a grain-boundary scattering term) and incorporate uniform softening (Fig. 3). In this

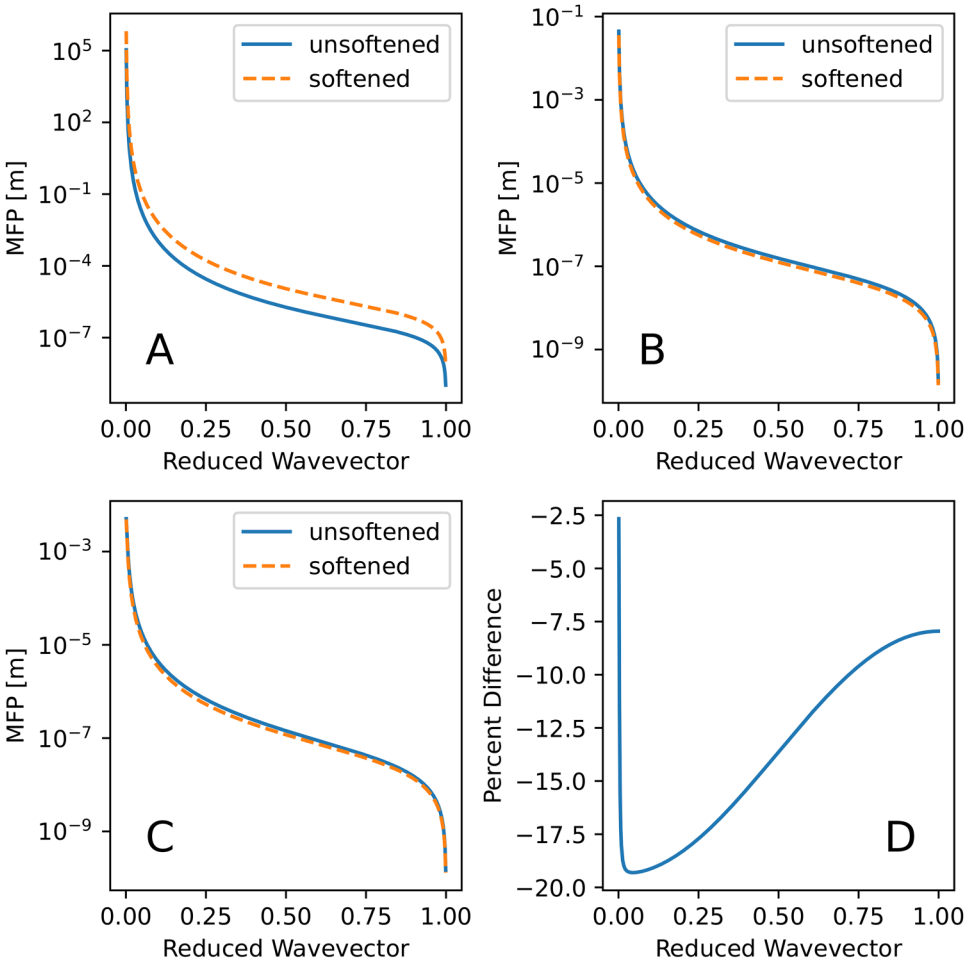

FIG. 3. MFP as a function of reduced wave vector for softened and un-softened silicon, $F_s = 0.44$ at 300 K, and this softening corresponds to a wire with a diameter of 20 nm. (a) Impurity scattering MFP term, (b) phonon–phonon scattering MFP term, (c) MFP from combined impurity and phonon–phonon scattering, (d) difference between softened and un-softened case in subfigure (c).

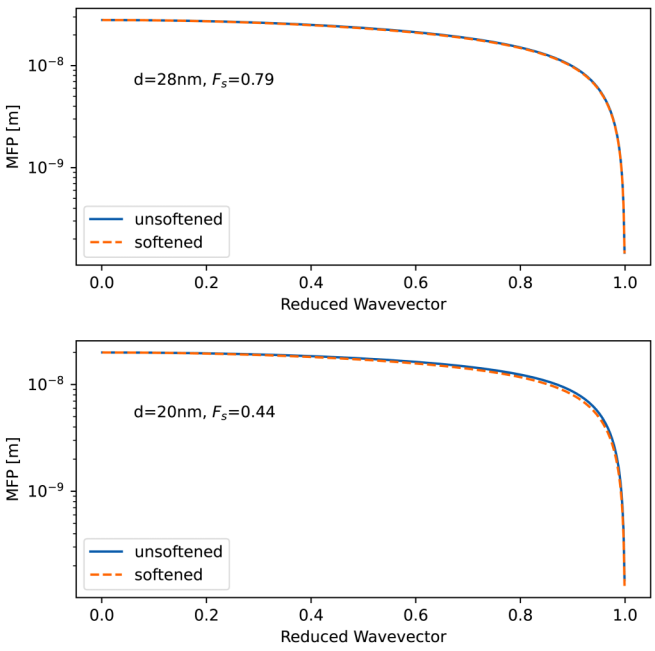

FIG. 4. Spectral MFP with and without softening (top) for a structure with a characteristic size of 28 nm and $F_s = 0.79$, and (bottom) for a structure with a characteristic size of 20 nm and $F_s = 0.44$.

system, the effects of phonon–phonon scattering dominate, and the MFP is reduced, by up to 20%. However, for the major portion of the FBZ, it is clear that the combined MFPs are much longer than the characteristic size of the nanostructures that we are interested in. For structures where we would see softening of this degree, we expect that surface scattering will occur on a size scale of around 10^{-8} m (10 nm), where the MFPs from the combined phonon–phonon and impurity scattering are on the order of approximately 10^{-8}–10^{-5} m.

To demonstrate the characteristics of softening effects on MFP as a function of wavevector in a structure with a sufficiently small characteristic size, we add boundary scattering to the MFP via Matthiessen's rule. This is akin to a round wire with a diameter equal to the characteristic size. For the structures that show softening experimentally, and which we wish to investigate, the characteristic size is between 20 nm and 40 nm. The effective MFP as a function of the reduced wavevector is plotted in Fig. 4. Since the shortest MFP component will dominate the total MFP, the inclusion of a nanoscaled surface scattering term results in that term dominating the MFP. Consequently, the influence of softening on the MFP is diminished. For a 28 nm characteristic size, the reduction in the MFP is less than 2% for all wavevectors. For a characteristic size of 20 nm, the reduction in the MFP never exceeds 12% for any wavevector.

C. Heat capacity

In addition to the scattering rate, a change in phonon frequency and thus in phonon energies, also affects the heat capacity.

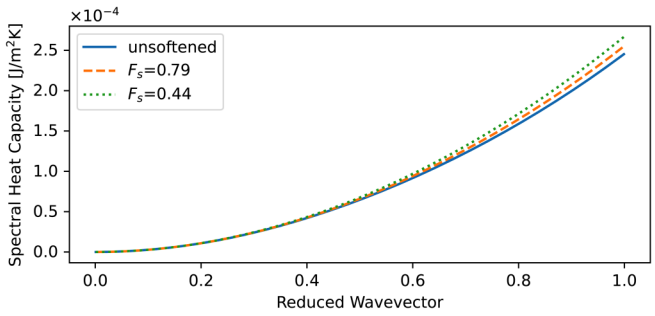

FIG. 5. Heat capacity as a function of reduced wavevector with and without softening.

In general, the reduction in the frequencies of phonons will result in a reduction in the energy of phonons with high wavevectors and thus an increase in the occupation of those states at a given temperature. Deriving a model for heat capacity using a spherical integration up to the cutoff wavevector, we have for each wavevector q,[36]

$$C_v(q) = \frac{3\hbar^2}{2k_B\pi^2}\frac{1}{T^2}\frac{q^2\omega^2(q)e^{\hbar\omega(q)/k_BT}}{(e^{\hbar\omega(q)/k_BT}-1)^2}. \quad (12)$$

Examining the spectral heat capacity across the FBZ, we see that softening should result in a slight increase in the spectral heat capacity, especially for longer wavevectors (Fig. 5). This increase is much smaller than the increase seen in the MFPs at room temperature.

As the heat capacity is responsible for a large portion of the temperature dependence of thermal conductivity, examining the temperature dependence of the heat capacity and the effect of softening on it become interesting. In Fig. 6, we plot the heat capacity as a function of temperature and note that there are significant changes on the heat capacity with softening. At low to intermediate temperatures, the heat capacity is significantly increased by the softening. This increase is mostly due to increased occupation numbers at low temperatures for the softened case, offsetting the

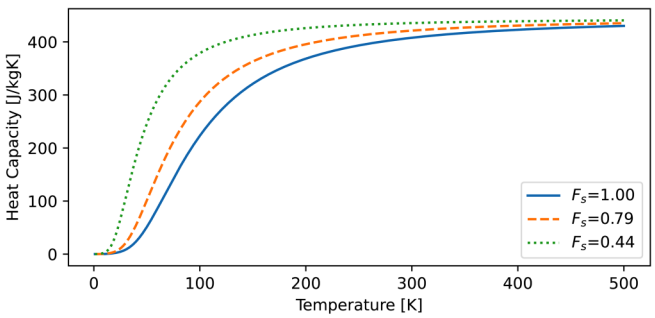

FIG. 6. Heat capacity as a function of temperature equivalent to 28 nm and 20 nm diameter wires ($F_s = 0.79$ and $F_s = 0.44$) and without softening.

decreased phonon energy. At higher temperatures, as expected, both heat capacities converge; at room temperature, the heat capacity is increased by 7% over the unsoftened case for $F_s = 0.44$.

III. DISCUSSION

While each of these factors contains interesting deviations from bulk and bulk-like values when acoustic softening is included, in order to see how acoustic softening should manifest in experimental measurements, we must combine these factors to calculate thermal conductivity.

Using as our example case a nanowire with a diameter of 20 nm and a softening factor of 0.44 [from Eq. (6)], we compute the spectral thermal conductivity. This example is of a similar scale to the first wires where anomalously low thermal conductivity was reported.[2] When we include the effects of softening on the heat capacity, phonon group velocity, and mean free path, we see that spectral thermal conductivity, instead of undergoing a flat reduction as seen for reducing the group velocity alone, The thermal conductivity reduction varies around the velocity-only value (Fig. 7).

While the contribution to thermal conductivity from longer wavelengths, where the difference in the softening models exists, is small, the overall change in the thermal conductivity between the two softening models is appreciable. For the model neglecting the effect of softening on the MFP and heat capacity, the thermal

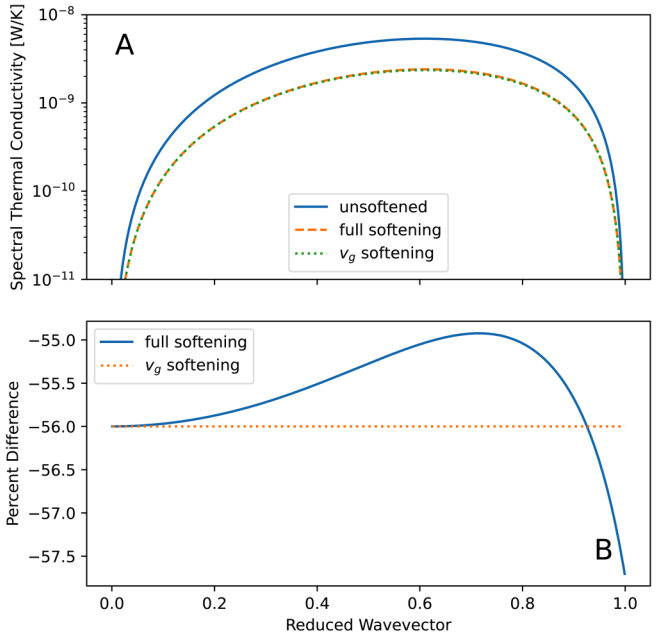

FIG. 7. (a) Spectral thermal conductivity as a function of reduced wave vector {i.e., thermal conductivity per inverse wave vector [W/(mK)/(1/m)]} for nanostructure with a characteristic size of 20 nm for unsoftened, v_g only softening, and softening including group velocity, MFP and heat capacity ($F_s = 0.44$). (b) Percent difference between the unsoftened and softened models.

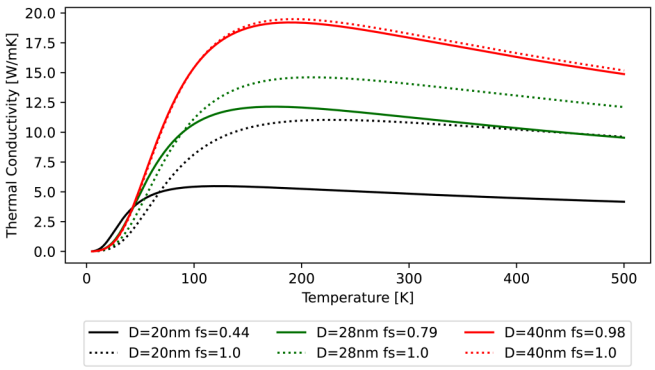

FIG. 8. Thermal conductivity as a function of temperature for a structures of various characteristic sizes with and without softening.

conductivity at this size scale is approximately 1.7% lower than the full softening model (4.76 W/m K vs 4.84 W/m K).

In addition to spectral thermal conductivity at room temperature, we can look at the temperature dependence of thermal conductivity under our softened model. In Fig. 8, we compare the softened and unsoftened thermal conductivity from the BvKS dispersion for 20–40 nm characteristic sizes with softening factors from Eq. (6). First, the change in the thermal conductivity is not uniform. While at higher temperatures, the thermal conductivity is reduced due to the softening, the low-temperature thermal conductivity (below about 75 K) is increased. Additionally, the temperature at which the peak thermal conductivity occurs is reduced. If softening were only affecting the group velocity of phonons, we would not expect to see these features, but rather a uniform shift of the thermal conductivity downward with temperature.

To further explore the origins of the changes in the temperature dependency, we consider the effects of each term in the kinetic theory independently on the temperature dependence of the thermal conductivity. In Fig. 9, we see that reducing the group velocity with a softening factor results in a uniform reduction across temperature. The other two factors in the thermal conductivity have significantly more variation over temperature. For the softening of the MFP, the effect on the thermal conductivity is to reduce the thermal conductivity slightly at higher temperatures, while little effect is seen at low temperatures. For the heat capacity factor, the thermal conductivity is increased by softening across all of the temperatures, but with the increase being mostly more dominant at lower temperatures and nearly disappearing by room temperature.

A. Comparison to experiment

To compare the results of our model with experiment, we focus on the results obtained Yang *et al.*[1] Here, thermal conductivity and elastic modulus were measured for two groups of nanoribbons with different thicknesses (a thick group between 30 and 32 nm thickness, and a thin group between 18 and 20 nm thickness). In each group, the width was varied, which varies the surface-to-volume ratio of the wire.

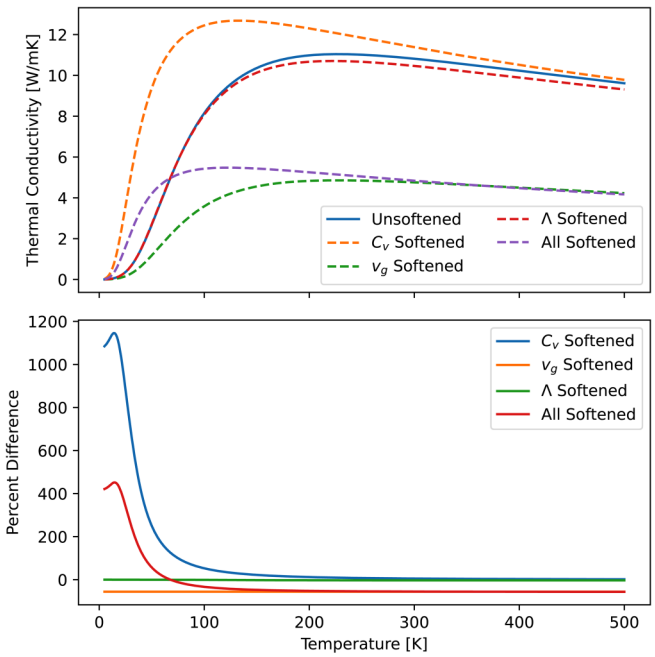

FIG. 9. Thermal conductivity as a function of temperature for a structure with a characteristic size of 20 nm ($F_s = 0.44$) with thermal conductivity from the components of the softening model plotted separately.

We have attempted to bracket the observed thermal conductivities with our MCRT model including a softening factor, F_s. In Fig. 10, thermal conductivities for wires with 20 nm and 30 nm thicknesses calculated with MCRT model with softening factors of 1.0 (unsoftened) and 0.44 (corresponding to a 20 nm diameter wire) are plotted with the experimental data. From this, we are able to model the thermal conductivity of the thick wires very well with an unsoftened MCRT model. However, the unsoftened MCRT models predict significantly higher thermal conductivity for the thin group of wires than observed.

For the thin group, we are able to bracket the data with our softened model using $F_s = 0.55$. This softening corresponds to a ratio of $E_{\text{nano}}/E_{\text{bulk}}$ of around 0.30, which is consistent with the maximum softening experimentally observed[19,20] and for a structure with a hydraulic diameter of approximately 22 nm using the data from Yang *et al.*[1] With this level of softening, we see that all of the ribbons in the thin group are bracketed by the MCRT.

Using F_s estimated from Eq. (6), MCRT simulations for both thick and thin ribbons are shown in Fig. 11. As the experimental ribbons have a thin oxide layer (approximately 2 nm thick[1]) that should play little role in thermal conductivity and that is not modeled in the MCRT simulations, 4 nm is removed from both the width and height of the ribbon when calculating the MFP with MCRT. With this model, we observe a close correspondence between the model and the experimental values.

While this model indicates that acoustic softening can explain the lower thermal conductivity for the thin group of wires, it does not explain fully the transition from unsoftened to softened that occurs with a move from the thick to thin ribbons. Some of the apparent sharpness may be geometric in nature, with the different thicknesses trending together for very small structures (high S/V), where the scattering is most strongly controlled by the width, but differing in the S/V regime where both thickness and width become important. Thus, the placement of the 1/(S/V) type curve for the thermal conductivities predicted is shifted to lower S/V ratios for thicker wires and to higher S/V ratios for larger wires.

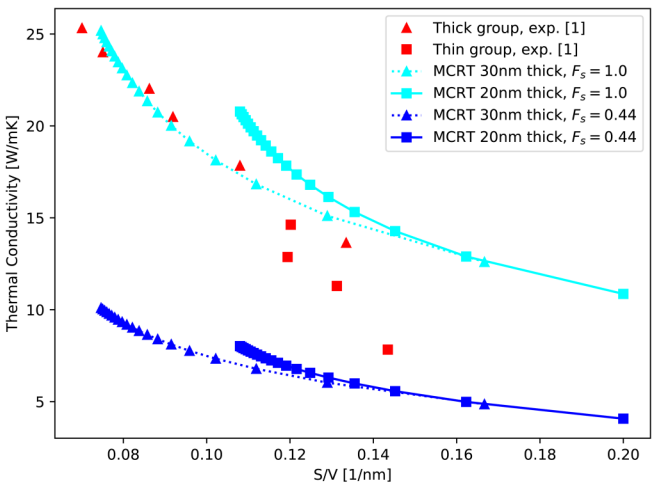

FIG. 10. Comparison of size sweeps of our thermal conductivity model with and without softening at 300 K to the thermal conductivity reported by Yang *et al.*[1] for nanoribbons at 300 K.

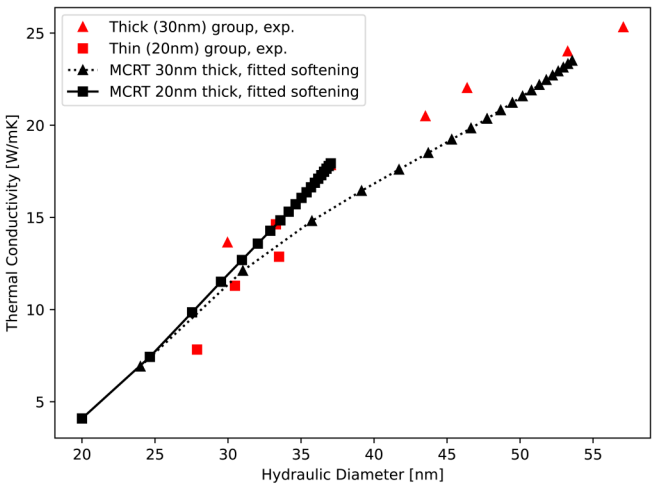

FIG. 11. Comparison of size sweeps using our thermal conductivity model with F_s given by Eq. (6) at 300 K with the thermal conductivity reported by Yang *et al.*[1] for nanoribbons at 300 K. For the ribbons from Yang *et al.*, 2 nm of oxide is discounted in the calculation of the hydraulic diameter.

Another factor affecting the apparent suddenness of the transition is the high degree of sensitivity of acoustic softening phenomena to such influences as surface recombinations,[9] the relative size of oxide layers,[13–15] and etching defects.[14,16] Computational work by Shim *et al.* has shown that the surface recombination of various silicon surfaces has a strong impact both on the magnitude of softening and the direction, indicating that for some recombinations a nanoscale stiffening can occur.[9]

While comparison to our model for the effect of acoustic softening on thermal conductivity with the size-dependent data gives us some confidence that our method produces results that match the general trends seen in experiment, it does not fully disentangle if softening effects in heat capacity and scattering are observed in the experimental data. However, because of the difference in the effects of softening at low and high temperatures, we examine the temperature-dependent thermal conductivity reported by Yang *et al.*[1]

In Fig. 12, we show thermal conductivity from MCRT for wires of the same sizes as Yang *et al.*, with F_s from Eq. (6). Again, when computing the MFP, the dimensions of the nanoribbons were reduced by 4 nm to account for the approximately 2 nm thick oxide commonly present in experiment. We calculate thermal conductivity using both a softened and unsoftened model and compare them to the data reported by Yang *et al.*[1] Importantly,

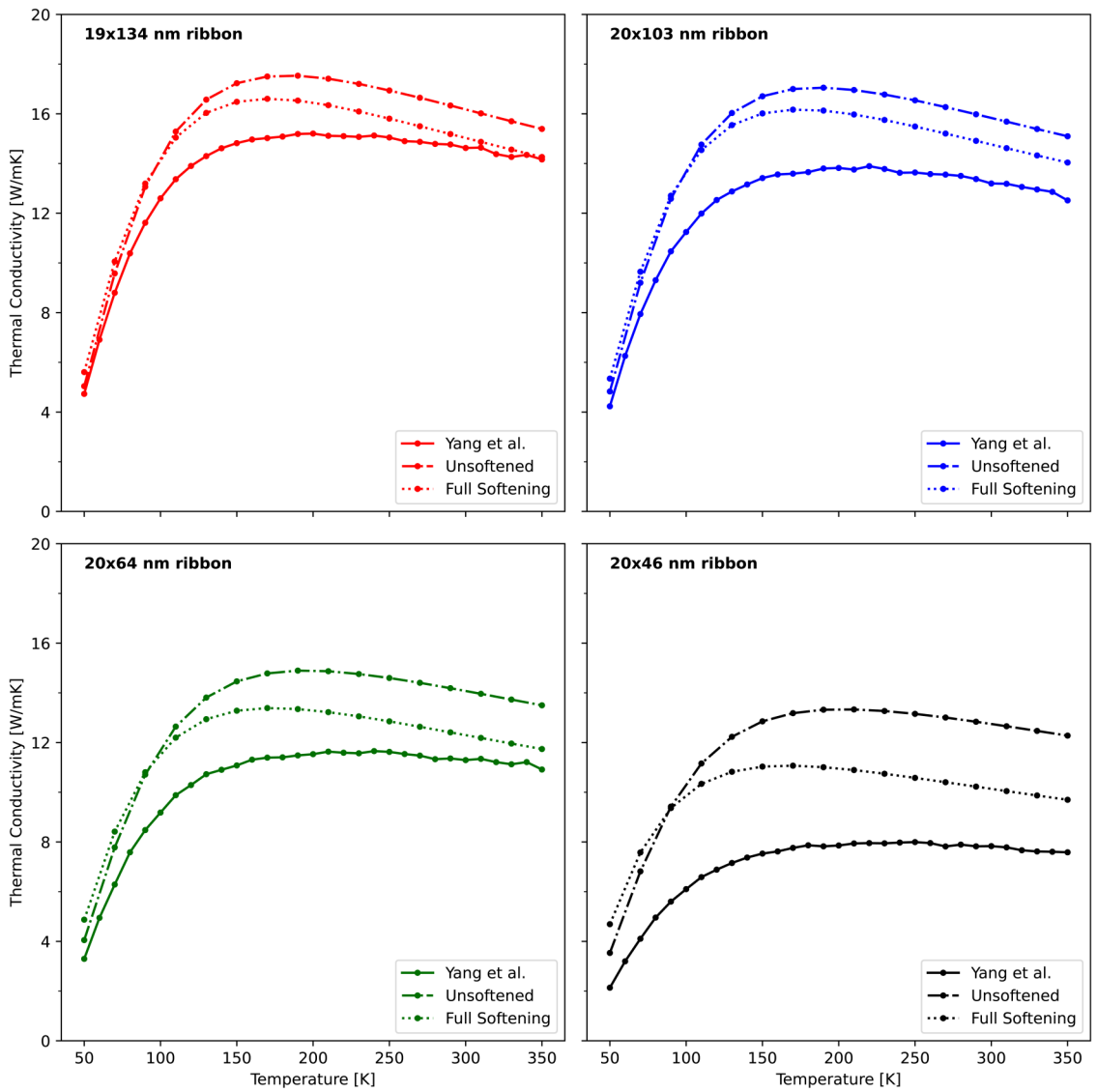

FIG. 12. Calculated thermal conductivity for wires with sizes matched to those reported by Yang *et al.*[1] without softening, with softening from Eq. (6).

including heat capacity and MFP effects in the softening shifts the peak thermal conductivity to lower temperature. At lower temperatures, the thermal conductivity is increased, while at higher temperatures, the thermal conductivity is decreased. This is similar to the effect seen for Ge–Si core-shell wires.[4]

When compared with the values reported by Yang *et al.* for the temperature-dependent thermal conductivity in thin wires, a few features are notable. First, there is a flatter dependence on temperature after the peak thermal conductivity in the reported values than for the softening model. In the reported values, Umklapp scattering begins to have a noticeable effect (i.e., thermal conductivity stops increasing rapidly) around 125–150 K. This is in contrast to a model including contributions from softened heat capacity and mean free paths where Umklapp scattering begins to dominate around 75–100 K.

We attribute the discrepancies between the models and experiment to the highly approximate nature of the dispersion relationship used and the softening method. In particular, the fitting parameters for phonon–phonon scattering and for impurity scattering are taken from bulk silicon and vary for the nanostructures considered due to the processing. The lack of normal scattering in the model may additionally reduce the accuracy of the model at low temperatures. Additionally, the model for F_s used here is based on Young's modulus measurements, is entirely empirical, and may not completely capture the pertinent physics related to transport properties. Moreover, in contrast to our assumption that the softening is uniform across the cross section of the nanostructures we consider, effects of the surface energy are likely to be strongest at the surface of the wire and decay toward the center of the wire. Therefore, the approximation of a uniform distribution of strain energy should be examined. Finally, the effects of the surfaces on dispersion relation of the wires may not be the same for both the transverse modes and the longitudinal modes; the effects of oxide layers on the effective elastic modulus are not the same for extension and bending.

IV. CONCLUSIONS

We have developed a model of acoustic softening that incorporates the effects of changes in the elastic modulus on components of thermal conductivity beyond the phonon group velocity. By considering how a change in the elastic modulus (and thus the continuum speed of sound) should impact the general form of the dispersion relation, we are able to extract the expected influence of softening on heat capacity and various scattering processes. Including these factors allows us to match the general size dependence of thermal conductivity for wires for which acoustic softening has been observed.

Our model indicates that acoustic softening should modify more than just the group velocity. In particular, the heat capacity should be increased at low temperatures, while the mean free path should be slightly reduced. This results in a shifting of the peak thermal conductivity to lower temperatures and an increase in the thermal conductivity at low temperatures. This is similar to effects seen in Ge–Si core-shell wires,[4] and the effect is likely to be important for the thermal conductivity at low temperatures and for wires with surface layers.

This model indicates that the influence of acoustic softening phenomena at the nanoscale implicates changes in the dispersion relation that occur on these scales. Incorporating more fine-grained predictions of how the dispersion relation should be modified by surface phenomena at the nanoscale should improve these results and increase the ability of thermal conductivity models to predict nanoscale thermal conductivity in size regimes where size-dependent elastic-modulus effects occur.

ACKNOWLEDGMENTS

Support for this work was provided by the National Science Foundation (NSF) (No. CBET-1403456).

REFERENCES

[1]L. Yang, Y. Yang, Q. Zhang, Y. Zhang, Y. Jiang, Z. Guan, M. Gerboth, J. Yang, Y. Chen, D. Greg Walker, T. T. Xu, and D. Li, "Thermal conductivity of individual silicon nanoribbons," Nanoscale **8**, 17895–17901 (2016).
[2]D. Li, Y. Wu, P. Kim, L. Shi, P. Yang, and A. Majumdar, "Thermal conductivity of individual silicon nanowires," Appl. Phys. Lett. **83**, 2934–2936 (2003).
[3]R. Chen, A. I. Hochbaum, P. Murphy, J. Moore, P. Yang, and A. Majumdar, "Thermal conductance of thin silicon nanowires," Phys. Rev. Lett. **101**, 105501 (2008).
[4]M. C. Wingert, Z. C. Y. Chen, E. Dechaumphai, J. Moon, J.-H. Kim, J. Xiang, and R. Chen, "Thermal conductivity of Ge and Ge–Si core–shell nanowires in the phonon confinement regime," Nano Lett. **11**, 5507–5513 (2011).
[5]M. C. Wingert, S. Kwon, M. Hu, D. Poulikakos, J. Xiang, and R. Chen, "Sub-amorphous thermal conductivity in ultrathin crystalline silicon nanotubes," Nano Lett. **15**, 2605–2611 (2015).
[6]R. E. Miller and V. B. Shenoy, "Size-dependent elastic properties of nanosized structural elements," Nanotechnology **11**, 139–147 (2000).
[7]H. Sadeghian, J. F. L. Goosen, A. Bossche, and F. Van Keulen, "Surface stress-induced change in overall elastic behavior and self-bending of ultrathin cantilever plates," Appl. Phys. Lett. **94**, 231908 (2009).
[8]K. Kang and W. Cai, "Size and temperature effects on the fracture mechanisms of silicon nanowires: Molecular dynamics simulations," Int. J. Plast. **26**, 1387–1401 (2010).
[9]H. W. Shim, L. G. Zhou, H. Huang, and T. S. Cale, "Nanoplate elasticity under surface reconstruction," Appl. Phys. Lett. **86**, 151912 (2005).
[10]B. Lee and R. E. Rudd, "First-principles calculation of mechanical properties of Si001 nanowires and comparison to nanomechanical theory," Phys. Rev. B **75**, 195328 (2007).
[11]H. Sadeghian, J. F. L. Goosen, A. Bossche, B. J. Thijsse, and F. Van Keulen, "Effects of size and surface on the elasticity of silicon nanoplates: Molecular dynamics and semi-continuum approaches," Thin Solid Films **520**, 391–399 (2011).
[12]B. Gong, Q. Chen, and D. Wang, "Molecular dynamics study on size-dependent elastic properties of silicon nanoplates," Mater. Lett. **67**, 165–168 (2012).
[13]M. J. Gordon, T. Baron, F. Dhalluin, P. Gentile, and P. Ferret, "Size effects in mechanical deformation and fracture of cantilevered silicon nanowires," Nano Lett. **9**, 525–529 (2009).
[14]H. Sadeghian, C.-K. Yang, J. F. L. Goosen, A. Bossche, U. Staufer, P. J. French, and F. van Keulen, "Effects of size and defects on the elasticity of silicon nanocantilevers," J. Micromech. Microeng. **20**, 064012 (2010).
[15]Y. Calahorra, O. Shtempluck, V. Kotchetkov, and Y. E. Yaish, "Young's modulus, residual stress, and crystal orientation of doubly clamped silicon nanowire beams," Nano Lett. **15**, 2945–2950 (2015).
[16]H. Sadeghian, H. Goosen, A. Bossche, B. Thijsse, and F. van Keulen, "On the size-dependent elasticity of silicon nanocantilevers: Impact of defects," J. Phys. D Appl. Phys. **44**, 072001 (2011).

[17]Y. Zhu, F. Xu, Q. Qin, W. Y. Fung, and W. Lu, "Mechanical properties of vapor liquid–solid synthesized silicon nanowires," Nano Lett. **9**, 3934–3939 (2009).
[18]C. C. Röhlig, M. Niebelschütz, K. Brueckner, K. Tonisch, O. Ambacher, and V. Cimalla, "Elastic properties of nanowires," Phys. Status Solidi (b) **247**, 2557–2570 (2010).
[19]X. D. Han, K. Zheng, Y. F. Zhang, X. N. Zhang, Z. Zhang, and Z. L. Wang, "Low-temperature *in situ* large-strain plasticity of silicon nanowires," Adv. Mater. **19**, 2112–2118 (2007).
[20]X. Li, T. Ono, Y. Wang, and M. Esashi, "Ultrathin single-crystalline-silicon cantilever resonators: Fabrication technology and significant specimen size effect on Young's modulus," Appl. Phys. Lett. **83**, 3081–3083 (2003).
[21]R. Chen, J. Lee, W. Lee, and D. Li, "Thermoelectrics of nanowires," Chem. Rev. **119**, 9260–9302 (2019).
[22]A. Ward and D. A. Broido, "Intrinsic phonon relaxation times from first-principles studies of the thermal conductivities of Si and Ge," Phys. Rev. B **81**, 085205 (2010).
[23]F. Yang and C. Dames, "Mean free path spectra as a tool to understand thermal conductivity in bulk and nanostructures," Phys. Rev. B. **87**, 035437 (2013).
[24]C. Dames and G. Chen, "Theoretical phonon thermal conductivity of Si/Ge superlattice nanowires," J. Appl. Phys. **95**, 682–693 (2004).
[25]H. Sadeghian, C. K. Yang, J. F. L. Goosen, E. Van Der Drift, A. Bossche, P. J. French, and F. Van Keulen, "Characterizing size-dependent effective elastic modulus of silicon nanocantilevers using electrostatic pull-in instability," Appl. Phys. Lett. **94**, 221903 (2009).
[26]M. Nasr Esfahani and B. E. Alaca, "A review on size-dependent mechanical properties of nanowires" Adv. Eng. Mater. **21**, 1900192 (2019).
[27]B. Bhushan and X. Li, "Micromechanical and tribological characterization of doped single-crystal silicon and polysilicon films for microelectromechanical systems devices," J. Mater. Res. **12**, 54–63 (1997).
[28]L. Yang, Q. Zhang, Z. Cui, M. Gerboth, Y. Zhao, T. T. Xu, D. G. Walker, and D. Li, "Ballistic phonon penetration depth in amorphous silicon dioxide," Nano Lett. **17**, 7218–7225 (2017).
[29]W. Park, D. D. Shin, S. J. Kim, J. S. Katz, J. Park, C. H. Ahn, T. Kodama, M. Asheghi, T. W. Kenny, and K. E. Goodson, "Phonon conduction in silicon nanobeams," Appl. Phys. Lett. **110**, 213102 (2017).
[30]E. Sondheimer, "The mean free path of electrons in metals," Adv. Phys. **1**, 1–42 (1952).
[31]K. Fuchs and N. F. Mott, "The conductivity of thin metallic films according to the electron theory of metals," Math. Proc. Cambridge Philos. Soc. **34**, 100 (1938).
[32]M. Asheghi, M. N. Touzelbaev, K. E. Goodson, Y. K. Leung, and S. S. Wong, "Temperature-dependent thermal conductivity of single-crystal silicon layers in SOI substrates," J. Heat Transfer **120**, 30 (1998).
[33]A. J. H. Mcgaughey and A. Jain, "Nanostructure thermal conductivity prediction by Monte Carlo sampling of phonon free paths," Appl. Phys. Lett. **100**, 061911 (2012).
[34]J. Callaway, "Model for lattice thermal conductivity at low temperatures," Phys. Rev. **113**, 1046–1051 (1959).
[35]M. Kazan, G. Guisbiers, S. Pereira, M. R. Correia, P. Masri, A. Bruyant, S. Volz, and P. Royer, "Thermal conductivity of silicon bulk and nanowires: Effects of isotopic composition, phonon confinement, and surface roughness," J. Appl. Phys. **107**, 083503 (2010).
[36]N. W. Ashcroft and D. N. Mermin, *Solid State Physics* (Brooks/Cole, Belmont, CA, 1976), pp. 453–463.